

Identification of the tetra-interstitial in silicon

B. J. Coomer, J. P. Goss, and R. Jones
School of Physics, The University of Exeter, Exeter EX4 4QL, UK

S. Öberg
Department of Mathematics, Luleå University of Technology, Luleå S-97187, Sweden

P. R. Briddon
Department of Physics, The University of Newcastle upon Tyne, Newcastle upon Tyne NE1 7RU, UK

First-principles computational methods are employed to investigate the structural, vibrational, optical and electronic properties of the self-interstitial aggregate, I_4 in silicon. We find the defect to be electrically active and identify it with the B3 EPR center. We also show that its properties are consistent with DLTS and optical spectra observed following implantation of silicon.

A crucial element is missing from our understanding of the behavior of silicon self-interstitials under annealing. Although substantial experimental [1] and theoretical [2] activity has provided an accepted model for the structure of the extended, interstitial related $\{311\}$ defects, little is known about the processes by which they form or degrade via small multi-interstitials (I_n). This is important as these processes are related to the transient enhanced diffusion (TED) of dopants [3], which leads to device degradation in heavy radiation environments. One important clue to understanding interstitial condensation lies with the B3 electron paramagnetic resonance (EPR) center which is classified as a simple interstitial aggregate [4]. In this letter we show that the tetra-interstitial (I_4) is responsible for the B3 EPR center. This assignment provides a vital link between small interstitial aggregates and extended defects.

Recently, evidence has emerged that the structure of small self-interstitial aggregates is markedly different from that of $\{311\}$ extended defects. The transient supersaturation of a system undergoing Ostwald ripening has been exploited to estimate the formation energies of small interstitial aggregates [5]. These experiments demonstrated that magic numbers exist for interstitial aggregates in the early annealing stage. I_4 and I_8 are found to be particularly stable with a transition at $n \gtrsim 10$ to a broad range of defects with the characteristic energy of $\{311\}$ condensates. Furthermore, optical studies [6] confirm this picture, indicating that a structural transformation from I_n clusters to $\{311\}$ defects occurs at $\sim 600^\circ\text{C}$.

Deep level transient spectroscopy (DLTS) studies of Si ion implanted silicon has provided further information on the early stages of the ripening process [7]. Two donor ($0/+$) levels at $E_v + 0.29$ eV and $E_v + 0.48$ eV associated with small interstitial clusters are found to dominate the DLTS spectrum before the emergence of a different signal at $E_v + 0.50$ eV. The latter level exhibits carrier capture kinetics typical of extended defects and is associated with $\{311\}$ condensates. The $E_v + 0.29$ eV level has been observed previously in carbon implanted silicon and is correlated with the B3 EPR center [8].

B3 is a prominent $S = 1/2$ center observed in boron doped, neutron irradiated and heat-treated silicon [4,9]. It is first observed upon annealing at $\sim 200^\circ\text{C}$ and completely anneals out at 500°C [9,4]. B3 is one of only eight defect centers observed in irradiated silicon which have been reported to possess D_{2d} symmetry and its stability to high temperatures suggests a simple secondary irradiation product of particularly low formation energy. The lack of low temperature stress response for B3 indicates that the D_{2d} symmetry does not result from a Jahn-Teller distortion [4]. Analysis of the hyperfine structure reveals further information about the defect structure: (i) The defect center is probably vacant. (ii) Two equivalent Si atoms lie along the principal $\langle 001 \rangle$ axis. (iii) Only 9% of the unpaired electron is localized on each of these two atoms. (iv) The electronic wavefunction on these atoms is predominantly p -like with only 6% s character.

Since the concentration of the defect is much larger than the oxygen or carbon concentrations in the samples used, the defect is assumed to be intrinsic. Additionally, no hyperfine interaction with impurity atoms could be detected. The defect is not thought to be vacancy related for two key reasons. Only V_1 and V_5 amongst the small vacancy aggregates could possess D_{2d} symmetry, but in conflict with the observation, this could only result from a distortion from tetrahedral symmetry. Secondly, vacancy defects possess hyperfine splitting character which reflects the high electron localization on $\langle 111 \rangle$ dangling bonds whereas the B3 spectrum in no way reflects this degree of localization.

The geometry of I_4 which we present here as a structural model for the B3 EPR center has been put forward previously. Originally, this geometry was presented as a candidate building block for extended defects observed in diamond [10]. It was subsequently suggested as a model for I_4 in silicon [11,12]. The latter proposal for this structure lacked experimental backing and the authors suggested that the absence of data consistent with the defect was due to its inert character. In this letter we demonstrate that the structure is electrically active and relate the center to experiment.

We analyze the interstitial defects within local density-functional theory (DFT) using both cluster-based (AIM-PRO [13]) and supercell methods. In the cluster approach the defect is positioned at the center of a cluster of crystalline silicon. The dangling bonds at the cluster surface are saturated using hydrogen atoms. The wave-function fitting basis consists of independent s and p Gaussian orbitals with four different exponents, placed at each Si site. A fixed linear combination of two Gaussian orbitals are sited on the terminating H atoms. In addition, s and p orbitals are placed at each Si–Si bond center to ensure good description of the Kohn-Sham states. The charge density is fitted with four independent Gaussian functions with different widths on each Si atom and three on the terminating H atoms. One extra Gaussian function is placed at each Si–Si bond center. In the supercell, the wave-function fitting method is the same as that for the cluster. The charge density is fitted with a plane-wave basis using a cut-off energy of 40 a.u. To calculate the electrical levels of I_4 , we compare the ionisation energy and electron affinity with those of the carbon interstitial. This is a proven technique [14] which circumvents problems associated with aligning the energy levels obtained from perfect and defective clusters or unitcells. The positions of all bulk atoms are optimized using a conjugate gradient method. Particular care is taken to ensure convergence of structures with cluster size. The I_4 defect structure is optimized in three clusters with configurations $\text{Si}_{88}\text{H}_{64}$, $\text{Si}_{188}\text{H}_{120}$ and $\text{Si}_{290}\text{H}_{144}$ and also in a Si_{100} supercell. The ideal Si-Si bondlength calculated using the cluster method is found to be smaller than the experimental value by just 0.1%.

We now consider the calculated properties of the optimized defect separately and relate the results to experiment.

Structure: The I_4 defect is constructed by replacing four next-nearest neighbour atoms which lie in a common $\{001\}$ plane with four $\langle 001 \rangle$ split interstitial pairs (Fig. 1). Optimization of the structure demonstrates that each atom pair forms bonds with the neighboring pairs, resulting in full four-fold coordination. The defect possesses symmetry operations [16] which identify it with the D_{2d} point group, consistent with the symmetry assignment of the B3 EPR center. We calculate that I_4^0 possesses bond lengths and bond angles close to their ideal values (2.35 Å and 109.47° respectively), in agreement with previous *ab initio* calculations [12]. In particular, the bond angle distortions in the defect core of I_4 relaxed in the $\text{Si}_{290}\text{H}_{144}$ cluster were found to be within the range -0.9 to -11.8% of the ideal bond angle compared with -1.3 to -13.2% found using a 196 atom supercell [12]. The bondlengths, given in Table I, are found to be within $\sim 5\%$ of the bulk value.

Electronic levels: The position of the donor level of I_4 was found by comparing the ionization energy of I_4 with that of the carbon-interstitial which has an experimentally determined donor level at $E_v + 0.28$ eV [17]. The calculations were performed in all three clusters and the I_4 ionization energy was found to be $0.01 - 0.12$ eV higher than that of the carbon-interstitial placing the I_4 donor level between $E_v + 0.16$ and $E_v + 0.27$ eV. This result is consistent with the correlation of the $E_v + 0.29$ eV hole trap with the B3 center [8]. No other electronic levels are calculated to lie within the band gap. This determination of an electrical level associated with I_4 is in contradiction with previous results [12] and is probably resultant from the more reliable electronic level calculation method employed here. The association of a donor level with this fully-coordinated structure may be expected as a result of the compressive strain in the defect core. The compression of bonds leads to increased interaction between sp^3 orbitals on next-nearest neighbors, increasing the valence band width and pushing states into the band-gap region. The donor activity then arises from these filled states displaced upwards from the valence band edge.

Paramagnetic properties: The presence of a donor level shows that the defect exists in the positive charge state. Whilst, in principle, a defect with D_{2d} symmetry could undergo a Jahn-Teller distortion, no such distortion is expected from I_4^+ as the highest occupied orbital is non-degenerate with a_1 symmetry. I_4 was optimized in the positive charge state and the bondlengths in the defect core were found to differ by less than 1% from those of the neutral defect.

The defect structure is wholly consistent with the interpretation of the nuclear hyperfine interaction data on B3 [4], having no atom present at the defect center and two equivalent atoms (labelled a in Fig. 1) lying along the principal $\langle 001 \rangle$ axis. The wavefunction occupied by the unpaired electron of I_4^+ is shown in Fig. 2. Clearly the unpaired wavefunction is spread over a number of atoms, whilst the largest amplitude lie near atom sites labelled a . Mulliken analysis shows that 6% of the unpaired wavefunction is localized near atom a in excellent agreement with the value obtained from ^{29}Si hyperfine measurements (9%). We also find that the unpaired electronic wavefunction is strongly p -like in character consistent with the 94% anisotropic component observed. Hyperfine splitting due to interaction with other nuclei is also observed in the B3 spectrum. These were not resolved and therefore no further detailed information regarding other nearby nuclei could be ascertained. The Mulliken analysis, however, shows that around 3% of the unpaired wavefunction is localized upon each site labelled b and another 3% is localized near the sites labelled c . It is probable that the unresolved hyperfine splitting is a result of interaction with nuclei at sites b or at c .

Stress response: An important characteristic of an anisotropic defect is the stress or piezospectroscopic tensor [18]. The energy of a defect within a strained crystal is $\Delta E = \text{Tr} \mathbf{B} \cdot \epsilon$ where \mathbf{B} is a traceless stress tensor. In the absence of any imposed stress, one third of the I_4 defects are aligned along each $\langle 100 \rangle$ axis. Imposing a tensile stress along $[001]$ lowers the energy of those I_4 centers with this orientation and, if the defect can reorientate, leads to a decrease

in the numbers of defect aligned along [100] and [010]. Experiment [4] shows that a stress of 180 MPa at 350°C along $\bar{[110]}$, leads to twice the number of B3 centers aligned along [001] as along [100] or [010] [19]. This gives a stress tensor whose principal directions coincide with the cube axes and whose principal values are $B_1 = B_2 = -B_3/2$ with $B_3 = -28$ eV. We have calculated this tensor by first relaxing the volume of a 100 atom unit cell containing the defect and then imposing a strain along the cube axes. We found $B_1 = B_2 = -B_3/2$ with $B_3 = -33$ eV. The negative value to B_3 means the defect exerts a considerable compressive stress along [001] as expected. The good agreement strongly supports the model for the B3 center.

Energetics: The formation energy of the I_4 defect, $E_f(I_4)$, relative to four bulk atoms was calculated using the supercell method to be 8.7 eV. Experimental determination of this energy gives a value of around $E_f(I_1) + 3.4$ eV [5]. We calculate $E_f(I_1)$, the formation energy of the isolated $\langle 110 \rangle$ orientated interstitial to be 3.9 eV. This brings the calculated formation energy of I_4 to $E_f(I_1) + 4.8$ eV, in agreement with experiment given the errors involved in both the theoretical and experimental determination of these values. The binding energy of I_4 relative to four separated $\langle 110 \rangle$ orientated interstitial atoms is calculated to be 6.9 eV.

The high thermal stability of B3 is explained by the low formation energy calculated for I_4 . This result is expected from the I_4 model because of the near ideal bonding arrangements of all atoms. The model also explains the finding that I_8 also possesses remarkably low formation energy [5]. Clearly, eight [001] split-interstitial pairs can be sited on a (001) plane resulting in the formation of two neighboring I_4 defects. It is likely that this $(I_4)_2$ defect will possess a lower formation energy per interstitial than two separated I_4 units due to the mutual strain relief interaction between the units. The large increases observed in the formation energies of the defects I_5, I_6, I_7 relative to I_4 and I_8 is also consequent from this model as these intermediate defects are unable to achieve full coordination.

Optical properties: The correlation of I_4 to experimental spectra may possibly be extended to observations in photoluminescence (PL) and absorption. The 1039.8 meV zero phonon line (labelled I_3 or X) is produced by neutron, proton or ion implantation between 230 and 530°C independently of carbon or oxygen doping [20] and has been classified as an intrinsic center [21]. As with the B3 EPR center, the X-center is suggested to have inherent D_{2d} symmetry from stress measurements and consideration of the vibronic bandshape [20]. For the reasons discussed above this symmetry assignment is inconsistent with the defect being a small vacancy cluster.

Isochronal annealing experiments show the 1039.8 meV zero phonon line intensity appears to increase at the expense of another zero phonon line labelled W. The W-optical spectrum is also classified as an intrinsic center and experiments suggest that is an interstitial rather than a vacancy aggregate [22,23]. This supports the identification of the X-center with I_4 and suggests that the W-center is a smaller aggregate, I_2 or I_3 which is the precursor to the I_4 defect.

Calculation of the matrix elements for dipole transitions between the defect states in the band gap region was performed. A number of transitions are allowed between near band edge states with radiative lifetimes around 1–5 μs . The fastest of these transitions occurs between states of b_2 and a_1 symmetry. The large $\langle 001 \rangle$ stress response indicates that the X-line transition involves a shallow excited conduction band state, and assuming that the PL arises from a bound exciton, the donor level is placed around $E_v + 0.1$ again consistent with our calculation (~ 0.20 eV but in conflict with the DLTS assignment to B3 [8]).

Vibrational properties: The compressed bonds in the defect core result in increased force constants which are expected to give rise to vibrational modes with frequencies above the maximum lattice frequency (523 cm^{-1}). Infra-red studies [24] of neutron damaged silicon show that two local mode peaks are indeed observed at 530 and 550 cm^{-1} which are attributed to intrinsic defects. These modes are observed following irradiation at 130°C and survive up to $\sim 550^\circ\text{C}$. The local vibrational modes of the optimized I_4 defect were calculated using the cluster method. A series of local modes were calculated to lie within 30 cm^{-1} of the calculated maximum lattice frequency (536 cm^{-1}). The two highest infra-red active modes possess frequencies 577 and 557 cm^{-1} .

In conclusion, we identify I_4^+ with the B3 EPR center observed in irradiated p -type silicon. Its formation circumstances, symmetry, structure, electronic character and stress response strongly support this assignment. The calculated electrical activity is consistent with the correlation of the B3 EPR center with the 0.29 eV DLTS signal. We tentatively link the X-optical center with the B3 EPR center and the optical properties of the I_4 defect are calculated to be in reasonable agreement with this assignment. We calculate the vibrational properties of I_4^0 and predict that the defect gives rise to a series of local modes lying close to the Raman edge. The structure of the I_4 center clearly excludes it as an embryo for aggregation of the $\{311\}$ defects. This marked structural difference between small aggregates and extended interstitial defects, however, is supported by optical, DLTS and transient supersaturation experiments.

RJ thanks the ENDEASD network for support. SÖ thanks TFR for financial support.

- [1] S. Takeda, Jpn. J. Appl. Phys. **30**, L639 (1991).
[2] J. Kim, J. W. Wilkins, F. S. Khan, and A. Canning, Phys. Rev. B **55**, 16186 (1997).
[3] D. J. Eaglesham, P. A. Stolk, H.-J. Gossmann, and J. M. Poate, Appl. Phys. Lett. **65**, 2305 (1994).
[4] K. L. Brower, Phys. Rev. B **14**, 872 (1976).
[5] N. E. B. Cowern *et al*, Phys. Rev. Lett. **82**, 4460 (1999).
[6] S. Coffa, S. Libertino, and C. Spinella, Appl. Phys. Lett. **76**, 321 (2000).
[7] J. L. Benton *et al*, J. Appl. Phys. **82**, 120 (1997).
[8] B. N. Mukashev, A. V. Spitsyn, N. Fukuoka, and H. Saito, Jpn. J. Appl. Phys. **21**, 399 (1982).
[9] D. F. Daly, J. Appl. Phys. **42**, 864 (1971).
[10] P. Humble, Proc. R. Soc. Lond. A **381**, 65 (1982).
[11] N. Aria, S. Takeda, and M. Kohyama, Phys. Rev. Lett. **78**, 4265 (1997).
[12] M. Kohyama and S. Takeda, Phys. Rev. B **60**, 8075 (1999).
[13] R. Jones and P. R. Briddon, Chapter 6 in *Identification of defects in semiconductors*, Vol 51A of *Semiconductors and semimetals*, edited by M. Stavola, Academic press, Boston, 1998.
[14] A. Resende, R. Jones, S. Öberg, and P. R. Briddon, Phys. Rev. Lett. **82**, 2111 (1999).
[15] R
[16] The D_{2d} point group is characterized by the following operations: $C_2, 2S_4, 2C'_2, 2\sigma_d$.
[17] L. W. Song, X. D. Zhan, B. W. Benson, and G. D. Watkins, Phys. Rev. B **42**, 5765 (1990).
[18] A. A. Kaplyanski, Opt. Spectrosc. **16**, 329 (1964).
[19] The intensity of the B3 EPR lines are related to the number of B3 centers orientated parallel (n_A) or orthogonal (n_B) to [001] by $I_A/(I_A + I_B) = 0.7n_A/(0.7n_A + n_B)$. This takes into account the dependence of the transition matrix element on direction of magnetic field.
[20] Z. Ciechanowska, G. Davies, and E. C. Lightowers, Solid State Commun. **49**, 427 (1984) and references therein.
[21] O. O. Awadelkarim *et al*, Phys. Rev. B **42**, 5635 (1990).
[22] G. Davies, E. C. Lightowers and Z. Cienchanowska, J. Phys. C: Solid State Phys, **20**, 191-205 (1987).
[23] M. Nakamura, S. Nagai, Y. Aoki and H. Naramoto, Appl. Phys. Lett. **72**, 1347 (1998).
[24] R. C. Newman, D. H. J. Totterdell, J. Phys. C:Solid State Phys. **8**, 3944 (1975).

TABLE I. Calculated bondlengths of I_4 . Bondlengths are given with reference to the the atom sites labelled in Fig. 1. Two inequivalent bonds interconnect atom sites labelled c and are distinguished by their direction ($\langle 001 \rangle$ or $\langle 110 \rangle$). For the largest cluster and the supercell the deviation from the ideal Si-Si bondlength (2.35 Å) is given.

Bond	Si ₁₈₈ H ₆₄	Si ₁₈₈ H ₁₂₀	Si ₂₉₀ H ₁₄₄	Si ₁₀₀ supercell
ab	2.27	2.26	2.27 (-3.4 %)	2.26 (-3.8 %)
bc	2.29	2.29	2.30 (-2.1 %)	2.28 (-3.0 %)
cc [001]	2.21	2.22	2.24 (-4.7 %)	2.25 (-4.2 %)
cc $\langle 110 \rangle$	2.39	2.34	2.36 (+0.4 %)	2.32 (-1.3 %)

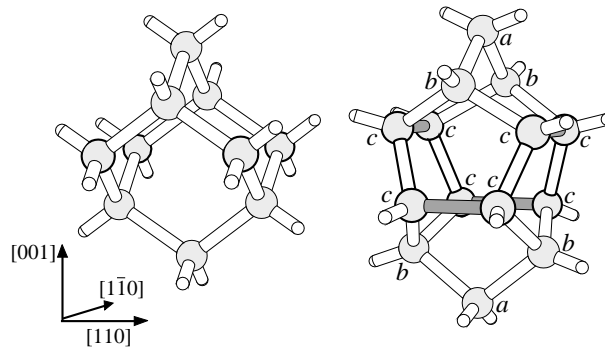


FIG. 1. Schematics showing the structure of I_4 . Left: A section of ideal silicon lattice. To form I_4 , four next-nearest neighbor atoms (shown in bold) are each replaced by [001] orientated atom pairs. Right: The fully optimized structure of I_4 in silicon. For clarity, the four [001] split interstitial pairs which make up the defect are shown in bold. The reconstructed bonds which link the interstitial pairs are shaded.

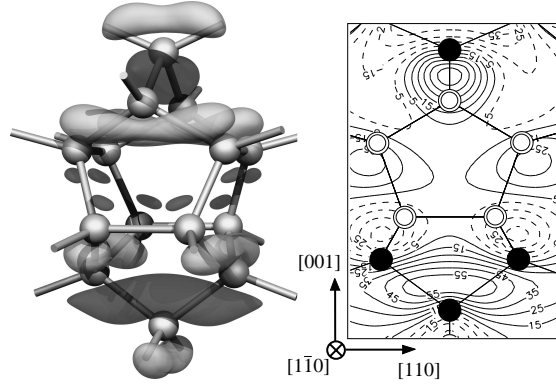


FIG. 2. Schematics showing the unpaired wavefunction of I_4^+ . Left: A 3-dimensional schematic of an isosurface of the wavefunction. Dark (light) surfaces indicate positive (negative) regions of the wavefunction. Right: Contour plot of the unpaired wavefunction on the $(\bar{1}\bar{1}0)$ plane. Contours representing positive (negative) regions are shown by solid (dashed) lines. Atoms lying in the plane are shown as black circles. Double circles indicate that two atoms lie equidistant from the plane along $[\bar{1}\bar{1}0]$ and $[110]$.